

Incorporation of thermally activated zeolite into carbon paste electrodes for voltammetric detection of carbendazim traces in milk samples

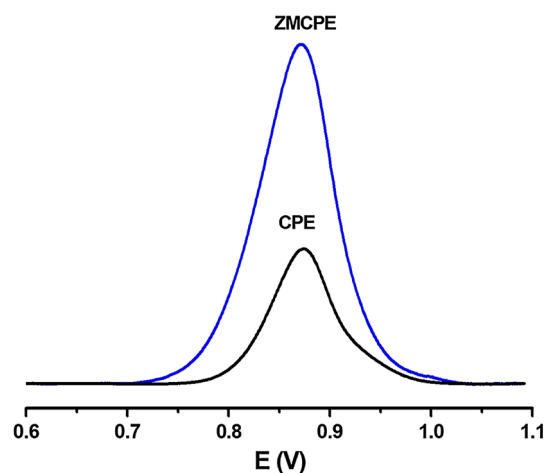
Elizabete Maria Maximiano¹ · Fábio de Lima² · Claudia Andrea Lima Cardoso¹ · Gilberto José Arruda³

Received: 28 July 2015 / Accepted: 8 December 2015 / Published online: 21 March 2016
© Springer Science+Business Media Dordrecht 2016

Abstract A simple, inexpensive, yet highly sensitive, and selective novel electrochemical method was developed to quantify traces of carbendazim (MBC) in soy milk and cow milk samples using previously thermally activated zeolite incorporated into carbon paste electrodes. Fourier-transformed infrared spectroscopy, scanning electron microscopy, and energy-dispersive X-ray spectroscopy were used to examine the structure of untreated and thermally activated zeolite, unmodified carbon paste electrodes, and zeolite-modified carbon paste electrodes (ZMCPEs). The electrodes were electrochemically characterized using cyclic voltammetry, square-wave voltammetry, and electrochemical impedance spectroscopy. The following electrochemical variables were measured: electrode area, number of transferred electrons, electron transfer

coefficient, standard rate constant of the electrode reaction, and capacitance of the electrical double layer. The electrocatalytic properties of zeolite were demonstrated by its strong influence on these variables when incorporated into carbon paste in both untreated and thermally activated forms. The electrochemical procedure applied to MBC was developed using ZMCPEs under optimal conditions. MBC oxidation currents exhibited linear concentration in the 12.9–777.7 nmol L⁻¹ range, with a limit of detection of 1.5 nmol L⁻¹. The proposed electrochemical method was employed to quantify MBC in soy milk and cow milk samples. Recovery rates were in the 98.6–99.8 % range, indicating that the method is applicable for quantifying MBC in such samples.

Graphical Abstract



Electronic supplementary material The online version of this article (doi:10.1007/s10800-016-0954-0) contains supplementary material, which is available to authorized users.

✉ Gilberto José Arruda
arruda@uem.br

¹ Graduate Program in Natural Resources, Universidade Estadual de Mato Grosso do Sul, Caixa Postal 351, Dourados, MS 79804-970, Brazil

² Institute of Chemistry, Universidade Federal de Mato Grosso do Sul, Caixa Postal 549, Campo Grande, MS 79070-900, Brazil

³ Chemistry Program, Universidade Estadual de Mato Grosso do Sul, Caixa Postal 351, Dourados, MS 79804-970, Brazil

Keywords Carbendazim · Zeolite · Thermal activation · Soy milk · Cow milk · Voltammetry

1 Introduction

Carbendazim, or methyl-2-benzimidazole carbamate (MBC, Fig. 1), is the active principle most widely employed in fungicide formulations of the benzimidazole carbamate class. Several methods have been reported for determining MBC content. Predominantly based on chromatography, these methods typically involve lengthy extraction steps and require expensive equipment [1–5].

Electrochemical methods for MBC analysis have received considerable attention, given their sensitivity, simplicity, and low cost. The literature reports a number of materials employed to modify the surface of glassy carbon electrodes (GCEs) for electrochemical quantification of MBC in different types of samples. Table 1 shows data on the electrodes, modifiers, samples, and limits of detection reported in a selection of these papers, briefly described below.

GCEs for MBC determination have been modified with a thin film of mesoporous silica/multi-walled carbon nanotubes [6], a functionalized carboxylic group [7], hybrid graphene oxide multi-walled nanotubes [8–11], cyclodextrin–graphene hybrid nanosheets [12], as polypyrrole-modified electrodes [13], montmorillonite clay–modified electrodes employed with surfactant [13, 14], boron-doped diamond electrodes [15, 16], and glassy carbon paste electrodes (GCPEs) modified with graphene and amberlite [17]. An electrochemical sensor based on graphene-printed electrodes has also been employed to this end [18].

Carbon paste electrodes (CPEs) can be easily prepared and used to detect oxidation or reduction of electroactive compounds adsorbed onto their surfaces [19]. CPEs using silicone oil and tricresyl phosphate as a binder were used to determine MBC by differential pulse voltammetry (DPV) [20, 21]. A sensor based on an ordered mesoporous CPE

modified with pyrrolidinium was developed for quantification of MBC in sugarcane by DPV [22]. Despite several published descriptions on the quantification of MBC in a variety of samples, no reports are available on electrochemical methodologies for determining MBC content in milk samples. In the present investigation, the electrochemical properties of MBC were investigated using a novel electrochemical method based on ZMCPEs prepared using thermally activated zeolite. CPE and ZMCPEs were characterized using cyclic voltammetry (CV), square-wave voltammetry (SWV), electrochemical impedance spectroscopy (EIS), infrared absorption spectroscopy (FTIR), scanning electron microscopy (SEM), and energy-dispersive X-ray spectroscopy (EDS). The proposed method was successfully applied to quantify MBC in soy milk and cow milk samples.

2 Experimental

2.1 Apparatus and reagents

2.1.1 Apparatus

All CV and SWV measurements were performed on an Autolab PGSTAT12 instrument (Eco Chemie, Utrecht, The Netherlands). The experiments were carried out in a three-electrode cell at room temperature (25 ± 1 °C), using a platinum wire as the counter-electrode, Ag/AgCl in KCl (3 mol L^{-1}) as the reference electrode, and ZMCPEs and an unmodified CPE as the working electrodes. The cell was placed in a Faraday cage to minimize background noise.

The EIS experiments, using a PGSTAT128 N potentiostat/galvanostat (Ecochemie, Utrecht, The Netherlands)

Fig. 1 Proposed mechanism of MBC oxidation

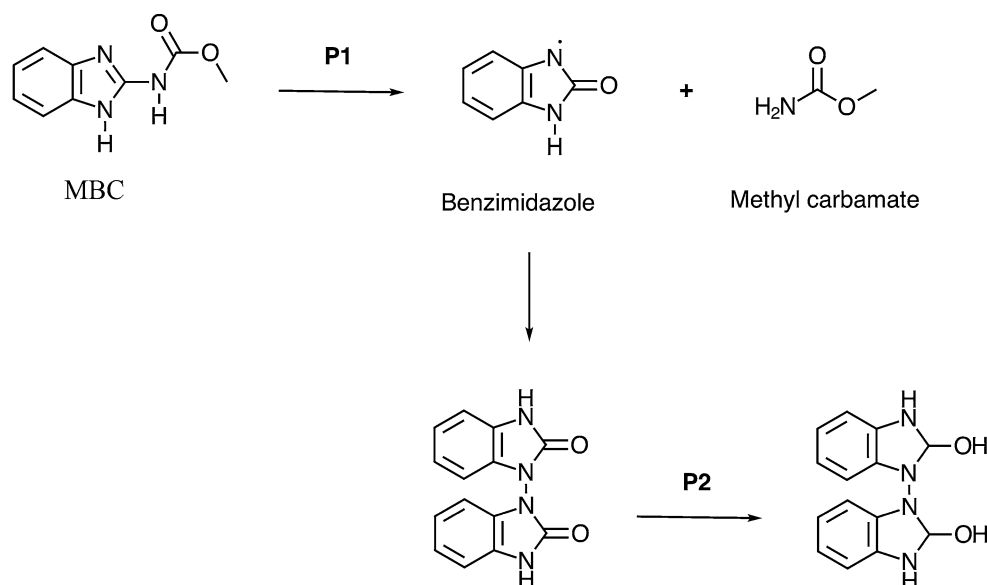


Table 1 Published electrochemical methods for quantification of MBC

Electrode	Method	Modifier	LOD (nmol L ⁻¹)	Sample	Ref.
GCE	SWV	SiO ₂ /MWCNT	56	Orange juice	Razzino et al. [6]
GCE	DPV	PC4-EDOT-COOH	3.5	Water and commercial juice	Yao et al. [7]
GCE	DPV	Graphene/MWCNT	5	Soil and tap water	Luo et al. [8]
GCE	SWV	MWCNT	55	River water	Ribeiro et al. [9]
GCE	DPV	MWCNT	0.05	Soil and water	Sundari et al. [10]
GCE	LSV	MWNT-PMRE	9	Distilled water	Li and Chi [11]
GCE	SWV	CD-GNs	2	Water	Guo et al. [12]
GCE	DPV	Acid Mont.	52	Soil and water	Manisankar et al. [13]
GCE	DPV	Na-Mont.	ND	Soil and water	Manisankar et al. [14]
DDB	SWV	SM	120	Waters: pure and natural	França et al. [15]
Screen-printed	SWV	Graphene	575	Water, soil, and vegetable	Noyrod et al. [18]
GCPE	DPV	GNS-XAD	3.1	Soil, fruit, blood serum, urine, waste, and ground water	Khare et al. [17]
CPE	DPV	UM	300	River water	Ashrafi et al. [21]
CPE	DPV	PIL/OMCPE	2.6	Sugarcane	Ya et al. [22]
CPE	DPV	SM	47.6	Wine, apple, and soil	Hernandez et al. [20]
CPE	SWV	Zeolite	1.5	Milk: soy and bovine	Present work

GCE glassy carbon electrode, DDB boron-doped diamond electrode. Screen-printed: carbon ink:grafite:graphene, CPE carbon paste electrode, SWV square-wave voltammetry, DPV differential pulse voltammetry, LSV linear sweep voltammetry, MWCNT carbon nanotubes multi-walled, PC4-EDOT-COOH carboxylic group functionalized poly (3,4-ethylenedioxythiophene, Na-Mont. sodium montmorillonite, Acid Mont. heteropolyacid montmorillonite, ND not determined, CD-GNs cyclodextrin graphene hybrid nanosheets, PMRE polymeric methyl red film, UM unmodified, PIL/OMCPE based on a pyrrolidinium ionic liquid (PIL)-modified ordered mesoporous carbon (OMC) paste electrode, GNS-XAD graphene nanosheets—Amberlite, GCPE glassy carbon paste electrode

equipped with a FRA2.X module, were performed at a fixed potential—namely, at an open-circuit potential (OCP) of 0.48 V (on average) in the presence of 5 mmol L⁻¹ K₃[Fe(CN)₆], with potential perturbation of 25 mV (rms) within a frequency range of 10 mHz to 100 kHz.

CV, SWV, and EIS were used for electrochemical characterization, measurement of electrical double-layer capacitance, calculation of the reactive surface area of the electrodes, and development of an analytical methodology for MBC quantification in milk samples. An HI 3221 pH-meter (Hanna Instruments) equipped with a glass electrode was employed for pH adjustments. Water purified in a Milli-Q system (Waters) was used as the sample for MBC quantification and to prepare the solutions.

CPE, ZMCPEs, and zeolite samples received an ultrathin deposited gold coating to ensure visualization of their microstructures by SEM, performed on a JSM-6380LV field-emission scanning electron microscope (JEOL) equipped with an EDS module. An accelerating potential of 20 kV was applied. FTIR transmittance spectroscopy was performed on a Bomen MB100 spectrophotometer equipped with a liquid-nitrogen-cooled MCT detector (Quebec, Canada), using a KBr pellet.

2.1.2 Reagents and solutions

Britton–Robinson (BR) buffers in the pH range of 4.0–8.0 were prepared by adding equal volumes of boric acid (Vetec), phosphoric acid (Synth), and acetic acid (Nuclear), each at 0.2 mol L⁻¹. Sodium hydroxide (Merck) at 0.2 mol L⁻¹ was employed to adjust the pH values. K₃[Fe(CN)₆] (Vetec) was employed as 2 (CV) and 5 (EIS) mmol L⁻¹ solutions; and KCl (Vetec) at 0.5 mol L⁻¹. All other reagents were of analytical reagent grade. Stock solutions of MBC (Sigma-Aldrich, 99.1 % purity) were prepared by dissolving this fungicide in an acetonitrile:H₂SO₄ (Vetec) (0.2 mol L⁻¹) (85:15; v:v) mixture. The working solution was prepared by diluting the stock solution in BR buffer at the desired pH.

2.2 Thermal activation of zeolite

Before mixing with graphite and Nujol for construction of the modified working electrodes, 5 g of zeolite was thermally activated by annealing in a porcelain crucible at 400, 600, 800, and 1000 °C for 2 h in an atmospheric environment.

2.3 Construction of CPE and ZMCPEs

CPE and ZMCPEs were prepared by mixing spectroscopic-grade graphite (Sigma-Aldrich, particle size <math><20\ \mu\text{m}</math>), Nujol (Sigma-Aldrich), and zeolite (Fluka, particle size $\leq 45\ \mu\text{m}</math>). The mixture was homogenized by hand in a glass mortar for 40 min and placed into a 1.0 mL plastic syringe with a geometric area of $0.054\ \text{cm}^2</math>. Electrical contact was established via a copper wire. The working electrodes were prepared with constant amounts of graphite powder (70 %) and Nujol (30 %) (CPE, 70:30, w:w), without modification. To prepare the modified electrodes, 29 % of zeolite was mixed with 50 % of graphite and 21 % of Nujol, without thermal activation (ZMCPE_x, 29:50:21, w:w:w) or with thermal activation at 400 °C (ZMCPE1), 600 °C (ZMCPE2), 800 °C (ZMCPE3), and 1000 °C (ZMCPE4). The surfaces of all electrodes were smoothed against weighing paper and carefully rinsed with distilled water.$$

2.4 Development of the new method and preparation of soy milk and cow milk samples

2.4.1 Using SWV to construct the analytical curve

Frequency, amplitude, step potential, and pH were the experimental and instrumental parameters optimized using CV and SWV. The values providing the best performance in terms of peak current intensity of MBC oxidation were employed to obtain the analytical curve (Table S1, supplementary data). To this end, suitable amounts of stock MBC solution at $57.5\ \mu\text{mol L}^{-1}</math> were diluted to 10 mL volumes with $0.2\ \text{mol L}^{-1}</math> BR buffer at pH 5 to yield concentrations of 12.97 to $777.92\ \text{nmol L}^{-1}</math>.$$$

2.4.2 Spiked soy milk and cow milk

Industrially processed soy milk and cow milk were acquired on the local market. After filtering the samples through cotton wool, 5 mL of each filtrate was spiked with MBC in amounts sufficient to yield concentrations of 42.4, 63.3, and $84.7\ \text{nmol/L}</math>. MBC recovery rates were determined by applying the addition method to the standard sample (three samples of soy and of cow milk were employed), using SWV and employing ZMCPE4 as the working electrode.$

3 Results and discussion

3.1 Electrochemical characterization of MBC using CPE and ZMCPEs

Figure 2 shows the SWV readings obtained with a CPE and a ZMCPE4 in the presence and absence of MBC at

$58.2\ \mu\text{mol L}^{-1}</math>. In BR buffer (curve *a*), no redox peak was observed for either electrode in the potential range of 0.4 to 1.2 V, indicating that ZMCPE4 was not electroactive in the scanned window. Highly sensitive anodic peak currents (I_p) of $30.14\ \mu\text{A}</math> (CPE, black I_r curve) and $99.98\ \mu\text{A}</math> (ZMCPE4, blue I_r curve) and a peak potential (E_p) of around 0.9 V were observed when MBC was added at $58.2\ \mu\text{mol L}^{-1}</math> to the BR buffer. The anodic peak current thus obtained for ZMCPE4 was 332 % higher than that for CPE, revealing the pronounced electrocatalytic activity of incorporated zeolite. Si–O–Al interactions present in the structure of zeolite cause charges to distribute onto the crystal structure—a distribution that depends on Al concentration. MBC interaction with zeolite occurs through this charge distribution, with increased electrocatalytic activity of ZMCPEs, compared with CPE.$$$$

According to the criteria for reversibility of an electrochemical reaction discussed by Osteryoung and Osteryoung [23] and Lovrić [24], the maximum current obtained in a square-wave voltammogram is given by the equation $I_r = I_f - I_b$, where I_f is the forward current (oxidation), I_b is the backward current (reduction), and I_r is the resulting current. I_r is obtained experimentally from the voltammogram, while I_f and I_b are calculated theoretically. The reversibility of the MBC redox process, which takes place on the electrode surface, was evaluated using CPE and ZMCPE4 and by employing SWV. As shown in Table 2, I_r roughly equals $I_f + I_b$. For both electrodes, a small shift can be observed at the 10 mV peak separation potential (ΔE_p). These results indicate that MBC oxidation occurs reversibly on CPE and ZMCPE4 surfaces.

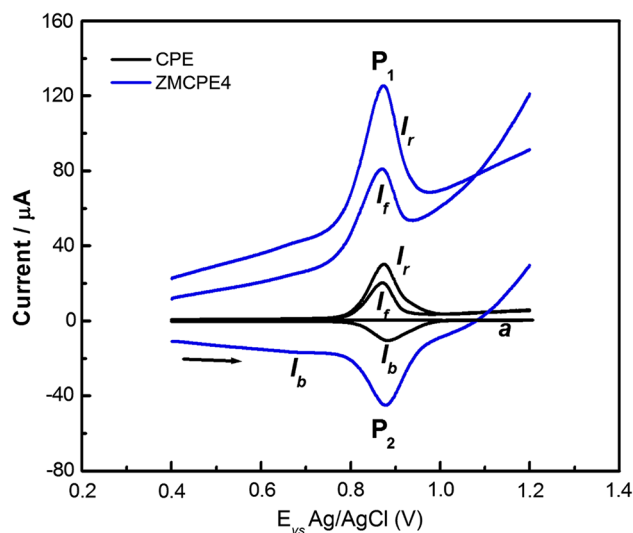


Fig. 2 SWV: CPE (black) and ZMCPE4 (blue), where I_f is the forward current (oxidation), I_b is backward (reduction), and I_r resultant current. $f = 30\ \text{Hz}$; step = 1 mV; and $a = 50\ \text{mV}$. (Color figure online)

The oxidation peak (P_1) shown in Fig. 2 was attributed to oxidation of the double bond of carbamate, involving two protons and two electrons and leading to formation of an amide (methyl carbamate: $\text{NH}_2\text{COOCH}_3$) and a heterocyclic radical [(3*H*,3'*H*-[1]bibenzimidazole)], which reacts with a similar radical, forming a dimer subsequently reduced (P_2) to the corresponding alcohol (Fig. 1) [13, 20].

The effect of pH on the electrochemical behavior of MBC was investigated using a 0.2 mol L⁻¹ BR buffer in the pH range of 4.0 to 8.0 and an MBC concentration of 57.5 μmol L⁻¹. Cyclic voltammograms using ZMCPE4 as the working electrode were recorded in the potential range of 0.4 to 0.1 to 1.2 V (Fig. S2A, supplementary data). Anodic (P_1) and cathodic (P_2) peak potentials were found to shift linearly toward more negative values with increasing pH values, indicating the intervention of protons in the electrochemical process of MBC (Fig. S2B, supplementary data). Adjusted by least squares, the potentials at P_1 and P_2 were found to vary linearly with pH, according to the following equations: $E_{p(P_1)}$ (V) = 1.172 - 0.058 ΔpH, $r = 0.998$, and $E_{p(P_2)}$ (V) = 1.132 - 0.060 ΔpH, $r = 0.999$. The slopes of the variations in E_p versus pH, of 0.058 V/ΔpH (P_1) and 0.060 V/ΔpH (P_2), suggest that the same numbers of protons and electrons are involved in the electrochemical oxidation of MBC, almost matching the theoretical Nernst equation [25]. The number of protons (m) can be calculated using the equation $\Delta E_p/\Delta \text{pH} = RTm/\alpha n$ [26]. Proton numbers were calculated as 2.2 (≈2) for P_1 and P_2 , respectively. Figure S2B depicts the variation of peak currents with pH, exhibiting maximum peak currents at pH 5.0, both for oxidation (P_1) and reduction (P_2). Based on these results, pH 5.0 was selected for the electrochemical study of MBC. For development of the analytical method, only the current at P_1 was optimized for MBC quantification.

For reversible reactions devoid of adsorption of redox reaction products, the relationship between peak potential variation and frequency variation is described by the equation: $\Delta E_p/\Delta \ln(f) = -R T/2n F$ (Fig. S3, supplementary data), where E_p is the peak potential, f is the frequency, n is the number of electrons involved in the reaction, R is the gas constant, and F is the Faraday constant [27]. This relationship was used to estimate the number of electrons involved in the oxidation of MBC (P_1) on the surfaces of

CPE, ZMCPE_x, and ZMCPE4, yielding values of 1.5, 1.8, and 1.9, respectively ([20]).

3.2 Influence of activation temperature on I_p in MBC oxidation

The effect of zeolite annealing temperature on the I_p value of MBC oxidation was evaluated by SWV using a 57.5 μmol L⁻¹ MBC solution in 0.2 mol L⁻¹ BR buffer (Fig. 3a). The peak current was found to rise with increasing annealing temperatures, up to 1000 °C (Fig. 3b). Thermal activation of zeolite prior to incorporation into the carbon paste increased the peak current by a factor of 3.3 compared with CPE and by a factor of 1.5 relative to ZMCPE_x.

3.3 Estimation of the electroactive area of CPE and ZMCPEs

For its chemical and electrochemical behavior, the Fe³⁺/Fe²⁺ couple is often adopted as a model system in electrochemical experiments [28]. In the present investigation, the couple was used to evaluate the performance of CPE and ZMCPEs employing CV in 2 mmol L⁻¹ K₃[(Fe(CN)₆], with 0.5 mol L⁻¹ KCl as the supporting electrolyte. The ratio between anodic and cathodic peak currents (I_{pa}/I_{pc}) obtained from the voltammograms (Fig. S4, supplementary data) was approximately 1, both for CPE and ZMCPEs, demonstrating the reversibility of the Fe³⁺/Fe²⁺ redox reaction [28]. According to the Randles–Sevcik equation [25], a linear relationship exists between the anodic and cathodic peak currents and the square root of the scan rate for mass transfer in reversible diffusion-controlled systems, as follows: $I_p = \pm 2.687 \times 10^5 n^{1.5} C D^{0.5} v^{0.5} A$, where I_p is the anodic (I_{pa}) or cathodic (I_{pc}) current peak (in amperes), n is the number of electrons involved, D is the diffusion coefficient ($6.39 \times 10^{-6} \text{ cm}^2 \text{ s}^{-1}$) [29], v is the scan rate (in V s⁻¹), and A is the electrode area (in cm²). The electroactive areas of the working electrodes (CPE, ZMCPE_x, ZMCPE1, ZMCPE2, ZMCPE3, and ZMCPE4) (Fig. S4, inset) were calculated using the slope of the I_p versus $v^{1/2}$ curve. The values thus obtained, of 0.045, 0.067, 0.087, 0.111, 0.115, and 0.121 cm², respectively, showed the electroactive area

Table 2 I_p and E_p values, obtained from voltammograms shown in Fig. 2

Electrode	I_p (μA)				E_p (V)			
	I_f	I_r	I_b	$I_r = I_f - I_b$	E_{pr}	E_{pf}	E_{pb}	$\Delta E_p = E_{pf} - E_{pb}$
CPE	30.14	19.22	-11.20	30.42	0.89	0.87	0.88	-0.01
ZMCPE4	108.19	55.49	-44.65	100.14	0.89	0.87	0.88	-0.01

I_f forward current, I_b backward current, I_r resultant current, E_{pr} forward peak potential, E_{pb} backward peak potential, E_{pr} resultant peak potential

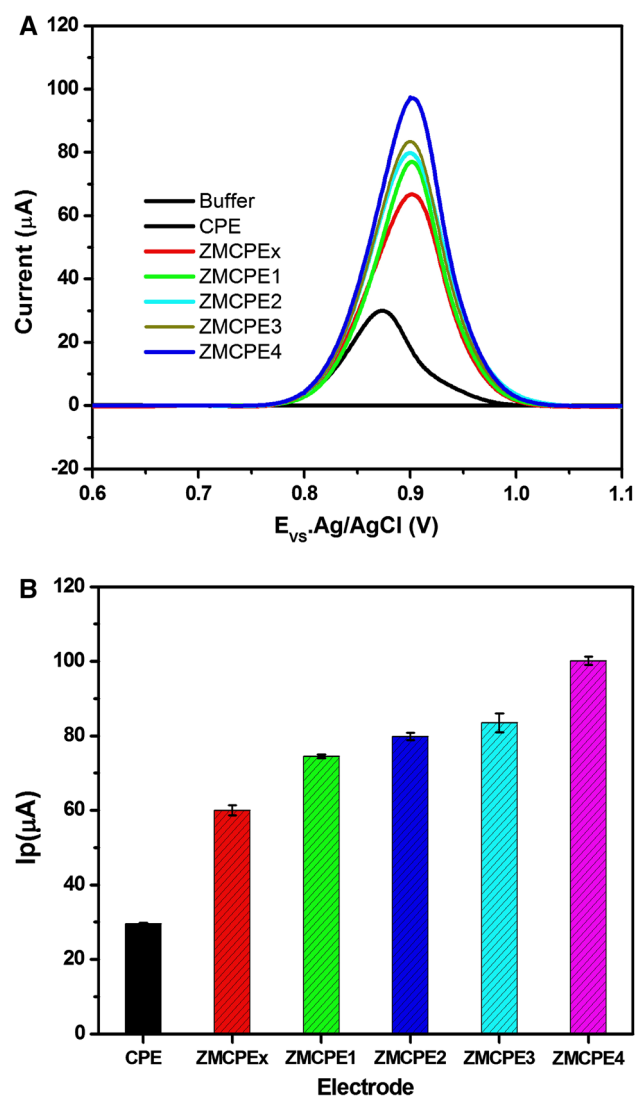


Fig. 3 **a** SWVs and **b** I_p versus type of electrode. [MBC] = 57.5 $\mu\text{mol L}^{-1}$; BR buffer in pH 5; f = 30 Hz; steep = 1 mV; and a = 50 mV

to be 183 % greater in ZMCPE4 than in CPE. Thermally activated zeolite increased the electroactive area of ZMCPE4 by more than 1.8 compared with ZMCPEx and by a factor of 2.7 relative to CPE. Incorporation of zeolite in the preparation of CPE increased the electroactive area of electrodes, leading to an increase in electrocatalytic activity during the oxidation of MBC on the electrode surface.

3.4 SEM and FTIR characterization of zeolite, CPE, and ZMCPEs

SEM images were used to investigate the surface structure and morphology of CPE (Fig. 4a, b), ZMCPEx (Fig. 4d, e), ZMCPE4 (Fig. 4g, h), thermally activated pure zeolite (Fig. 4j, k), and untreated pure zeolite (Fig. 4m, n). Clear

morphological differences were observed between CPE and ZMCPEs, demonstrating the effect of zeolite incorporation. Cubic crystals with sharp edges, sharp apexes, and uniform size of about 2 μm , typical of this material [30, 31], and particularly of NaA-type zeolites [32], were present (Fig. 4). The chemical composition of each sample was determined by EDS (Fig. 4c, f, i, l, o), revealing the presence of carbon, sodium, oxygen, silicon, and aluminum, with a Si:Al ratio of 1:1, suggesting a NaA-type zeolite [33].

Figure 5 shows the FTIR spectrum of untreated zeolite (Fig. 5a, Ze), zeolite thermally activated at 1000 $^{\circ}\text{C}$ for 2 h (Fig. 5a), CPE (Fig. 5b), ZMCPEx (Fig. 5b), and ZMCPE4 (Fig. 5b). For untreated zeolite, absorption bands were observed at 3425 and 1640 cm^{-1} , related to stretching vibration of the hydroxyl group in H-OH molecules entrapped in the zeolite structure [34]. The strongest band, at 1000 cm^{-1} , and another, less pronounced, at 870 cm^{-1} , corresponded to the internal stretching vibrations of Si-O(Si) and Si-O(Al) of zeolite tetrahedrons, respectively [35]. The band appearing at 760–660 cm^{-1} corresponded to quartz in the sample, whereas the band at 575–525 cm^{-1} indicated mullite in the zeolite structure (Fig. 5a, insert) [36]. The FTIR spectrum obtained for thermally treated zeolite was similar to that obtained for the untreated material. A decrease in band intensity at 3425 and 1640 cm^{-1} was evident, which can be attributed to loss of water molecules from the zeolite; an offshoot of the band at 575–525 cm^{-1} was also observed (Fig. 5a, insert). The unfolding of the absorption band may be ascribed to Al atoms being replaced with Si atoms by the effect of the rising temperature. This band is related to the presence of a double ring and found for all zeolite structures that contain double 4- and double 6-rings [37]. The absorption bands at 2920, 280, 1460, and 1360 cm^{-1} in the spectrum obtained for CPE (Fig. 5b) were attributed to absorption of C-H bonds resulting from axial and angular deformations of Nujol [38]. In the spectra of ZMCPEs (Fig. 5b), characteristic absorption bands of zeolite (1000, 720, and 550 cm^{-1}) and Nujol (2920, 2860, 1460, and 1360 cm^{-1}) were present, confirming the incorporation of zeolite into ZMCPEs.

3.5 EIS characterization of CPE and ZMCPEs

The electrocatalytic properties of CPE and ZMCPEs were investigated in EIS experiments (Fig. 6) employing 0.5 mol L^{-1} KCl containing 5 mmol L^{-1} of $\text{K}_3[\text{Fe}(\text{CN})_6]$. Cell resistance (R_s), charge transfer resistance (R_{ct}), double-layer capacitance (C_{dl}), and standard heterogeneous rate constant (k^0 or k_{app}^0) were the variables measured at an open-circuit potential (OCP). Nyquist plots (as semicircles from high to medium frequencies and straight lines at low

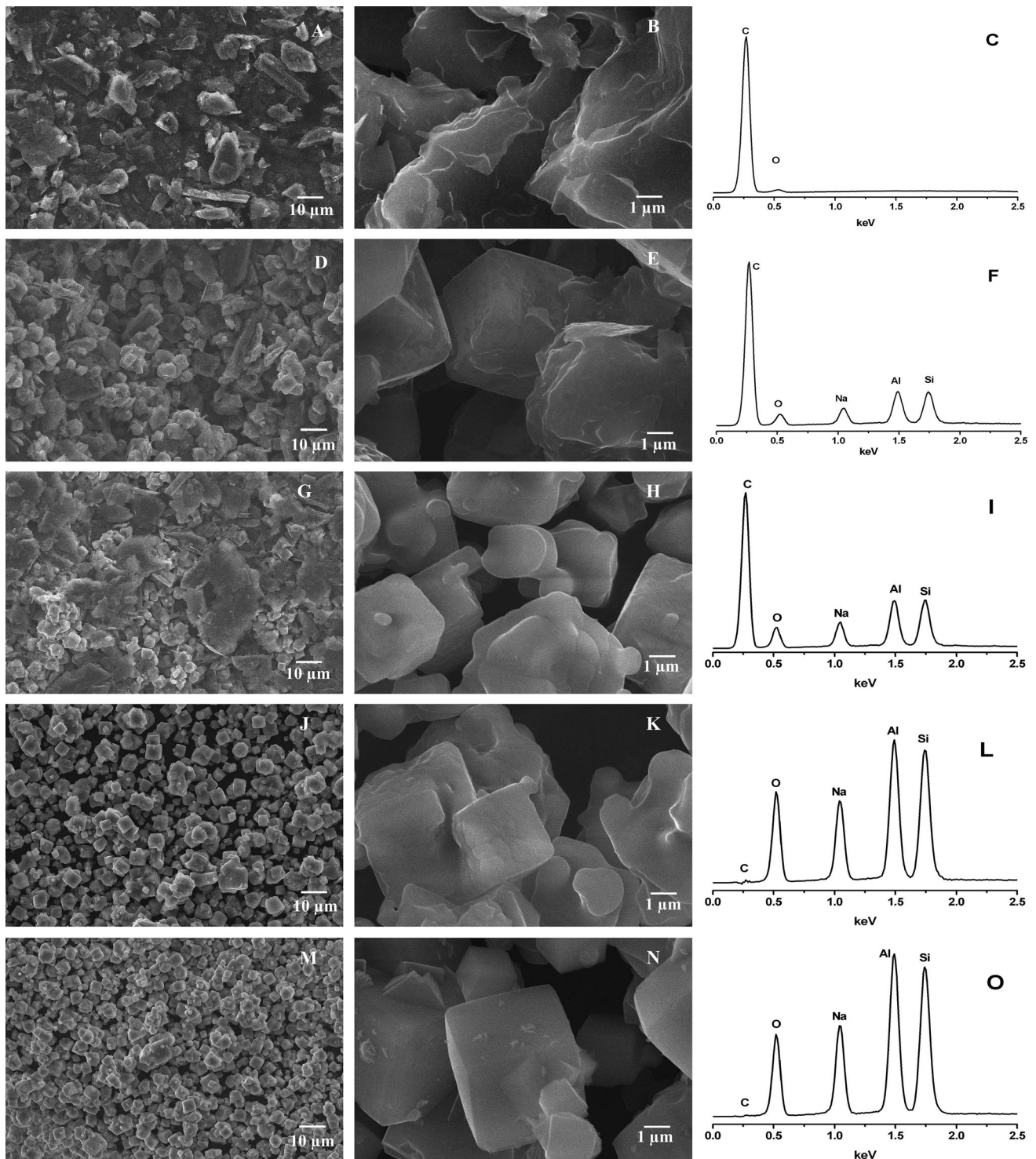


Fig. 4 SEM: CPE (a, b), ZMCPEx (d, e), ZMCPE4 (g, h), Zeolite thermally activated at 1000 °C (j, k), and native zeolite (m, n). EDS: CPE (c), ZMCPEx (f), ZMCPE4 (i), zeolite thermally activated at 1000 °C (l), and native zeolite (o)

frequencies, corresponding to kinetic and diffusion control, respectively) are depicted in Fig. 6.

The spectra shown in Fig. 6 were modeled using a modified Randles equivalent circuit (Fig. 6, insert), where R_s is the cell resistance, R_{ct} is the charge transfer resistance,

C_{dl} is the double-layer capacitance, and α is an exponent ($\alpha = 1$ represents a perfectly adjusted circuit; experimental data are related to the electrode surface), with a Warburg impedance (W , which takes into account mass transport limitations) resulting from the diffusion of the species

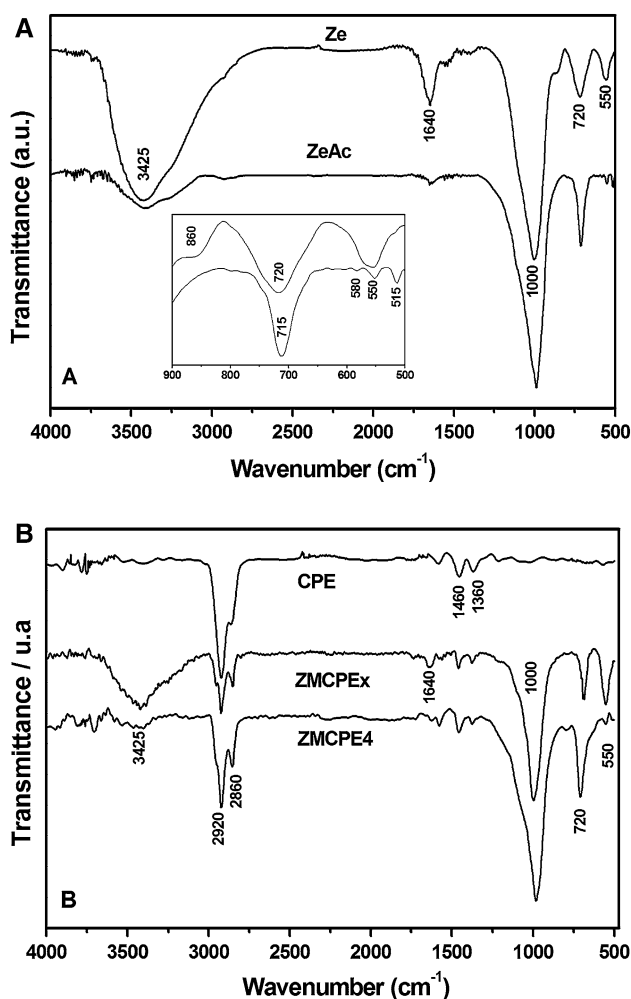


Fig. 5 FTIR. **a** Native zeolite (Ze) and zeolite thermally activated at 1000 °C (ZeAc). **b** CPE, ZMCPE_x, and ZMCPE₄

$\text{Fe}^{3+}/\text{Fe}^{2+}$ to the electrode surface. Post-adjustment values, shown in Table 3, reveal that incorporation of untreated or thermally activated zeolite changed the R_s , R_{ct} , C_{dl} , and k_{app}^0 values of CPE and ZMCPEs.

Zeolite incorporation into CPE and ZMCPEs increased R_s by 25 %, but no significant differences were observed between the use of untreated and thermally activated zeolite (Table 3). The increase was probably related to loss of mobility of Na^+ ions present in the material's composition, since heat treatment affects pore size [39]. A significant decrease in R_{ct} was observed when either type of zeolite was incorporated (Table 3), a feature that can be attributed to the conductive properties of this material (more pronounced than those of graphite), loss of water molecules, and morphological changes in zeolite upon incorporation into carbon paste. The increases observed in C_{dl} (Table 3) can be attributed to the greater electroactive area of the

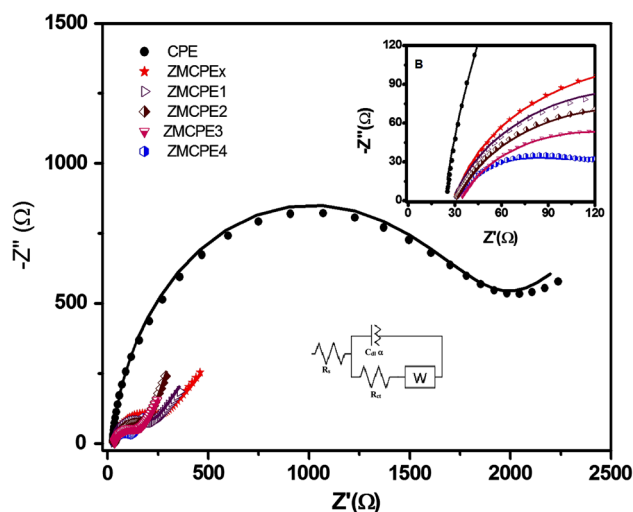


Fig. 6 EIS (Nyquist) CPE, ZMCPE_x, ZMCPE₁, ZMCPE₂, ZMCPE₃, and ZMCPE₄. Insets: Amplification of the high-frequency region and Randles equivalent circuit modified

modified electrodes (Sect. 3.3). The value of α declined from CPE to ZMCPE₄, probably owing to increasing surface roughness on the electrodes [40].

The standard heterogeneous rate constants were determined using the relationship $k_{app}^0 = R T/F^2 R_{ct} A C$, where R is the universal gas constant, A is the electroactive area of the electrode, T is the absolute temperature, n is the number of electrons involved in the electrode reaction, F is the Faraday constant, and C is the species concentration in the solution [41]. The values obtained, shown in Table 3, revealed that incorporating zeolite (whether untreated or thermally activated) increased k_{app}^0 , facilitating the action of the $\text{Fe}^{3+}/\text{Fe}^{2+}$ redox couple.

3.6 Linear range and limit of detection

To develop the methodology to be employed with ZMCPE₄, the following instrumental and experimental parameters were optimized with regard to the current at P_1 (oxidation): frequency, amplitude, step potential, and pH (Table S1, supplementary data). For its high sensitivity and limit of detection (LOD), SWV was the electrochemical method selected for MBC quantification under optimized conditions. The calibration curve (Fig. 7) exhibited good linearity for I_p versus MBC concentration was in the 12.97–777.72 nmol L^{-1} range. The linear equation obtained was I_p (μA) = 0.092 (μA) + 0.006 (nmol L^{-1}) [MBC], with $r = 0.999$. A LOD of 1.5 nmol L^{-1} was established using the relationship $\text{LOD} = 3 \text{SD}/s$, where s is the slope of the calibration curve and SD is the standard deviation of the mean value of currents, determined at the

Table 3 Summary of calculated EIS parameters obtained for the CPE and ZMCPEs

Electrode	R_s ($\Omega \text{ cm}^{-2}$)	R_{ct} ($\text{k}\Omega \text{ cm}^{-2}$)	C_{dl} ($\mu\text{F cm}^{-2}$)	α	k_{app}° ($10^{-5} \text{ cm s}^{-1}$)
CPE	454.28	30.48	9.94	0.94	3.25
ZMCPE _x	563.85	4.66	67.72	0.84	21.15
ZMCPE1	557.96	3.72	85.08	0.82	26.50
ZMCPE2	556.11	3.48	227.11	0.77	28.33
ZMCPE3	593.55	2.64	248.33	0.76	37.33
ZMCPE4	592.04	1.84	303.29	0.75	53.58

same potential as the peak for 10 voltammograms of blank (buffer solution at pH 5), according to IUPAC recommendations [42].

3.7 Interference

Interference studies were conducted to acquire information on the selectivity of ZMCPE4 in the presence of potential interferents. The possibility of inorganic ions interfering with the peak current (I_p) of MBC oxidation (P_1) was evaluated for Na^+ , Ca^{+2} , Mg^{2+} , Al^{3+} , and Cl^- , using MBC-to-ion ratios of 1:1000. Interference levels of less than 1.50 % were found. The applicability of the proposed method to quantify pesticides capable of interfering with the measurement of peak currents (P_1) was evaluated for atrazine (1:10 MBC-to-interferent ratio), linuron (1:10), glyphosate (1:10), thiamethoxam (1:10), and trifluralin (1:10). None of these ions and pesticides were found to affect MBC quantification (Table S5, supplementary data).

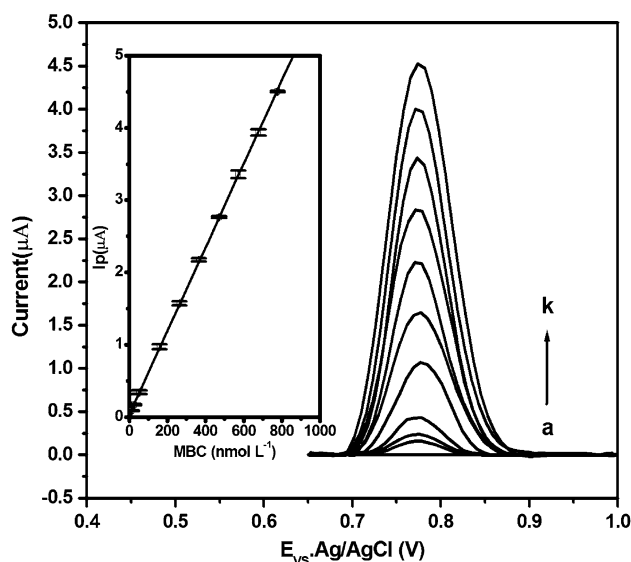


Fig. 7 SWV of MBC using ZMCPE4 in 0.2 mol^{-1} BR buffer at pH 5.0. [MBC] = 12.97, 25.94, 52.78, 158.26, 263.70, 364.80, 470.29, 571.39, 676.83, and 777.72 nmol L^{-1} . Inset: I_p versus [MBC]

3.8 Reproducibility, repeatability, and stability of ZMCPE

Repeatability, reproducibility, and stability are three important aspects of any determination method. Repeatability was determined in recovery experiments using three different preparations of the same sample. The results showed good recovery rates, of 98.6–99.3 %. Reproducibility was determined in three experiments performed at 1, 7, and 14 days. The results showed a relative standard deviation not exceeding 1.9, indicating good reproducibility. Additionally, electrode stability was also investigated, revealing that for electrodes stored in air at room temperature for 7 and 14 days, peak currents retained 98–99 % of their original responses.

3.9 Application of the proposed method to cow milk and soy milk samples

MBC recovery experiments were performed by adding known amounts (42.4 , 63.3 , and 84.7 nmol L^{-1}) to samples of cow milk and soy milk. ZMCPE4 was employed under the conditions optimized by SWV (Table S1). By applying the curve and standard addition methods (Fig. S6A and S6B, supplementary data), recovery rates of 98.3–99.8 % were obtained, with relative errors of less than 2 % (Table 4), demonstrating the feasibility of the proposed electrochemical method.

4 Conclusion

The incorporation of zeolite, whether thermally activated or untreated, increased the electrocatalytic activity of the modified electrodes investigated, relative to bare CPE. Two factors can explain this increase: (1) an enlargement of the electrochemical area of the modified electrodes, as a result of zeolite incorporation, and (2) the conductive properties of the electrode–solution interface: electron transfer resistance, double-layer capacitance, and the standard heterogeneous rate constant were strongly affected by the presence of zeolite in the electrodes. Combined, these

Table 4 Spiked and found amounts and recovery rates of MBC in cow milk and soy milk samples ($n = 3$)

Samples	Spiked (nmol L ⁻¹)	Found (nmol L ⁻¹) ^a	SD	RSD (%)	Recovered (%) ^b
Cow milk	42.4	42.1	0.6	1.4	99.3
	63.3	62.4	1.0	1.6	98.6
	84.7	84.0	1.3	1.6	99.2
Soy milk	42.4	42.1	0.6	1.4	99.3
	63.3	62.8	0.7	1.1	99.2
	84.7	83.7	1.6	1.9	98.8

RSD relative standard deviation, SD standard deviation

^a Average of five measurements

^b Amounts and percentages of recoveries by standard addition method the sample

factors caused the MBC oxidation peak current to rise on the surface of the zeolite-modified electrodes, imparting higher sensitivity to the proposed electrochemical method. Under optimized conditions, the method yielded a lower LOD than other techniques reported in the literature. MBC recovery rates of 98.3–99.8 % were achieved, both for soy milk and cow milk samples.

Acknowledgments The authors wish to thank FUNDECT-MS, CAPES, FINEP, and CNPq for the grants awarded. Thanks are also extended to the Institute of Physics and the Institute of Chemistry of the Universidade Federal de Mato Grosso do Sul for the SEM and FTIR measurements, respectively.

References

- Boeris V, Arancibia JA, Olivieri AC (2014) Determination of five pesticides in juice, fruit and vegetable samples by means of liquid chromatography combined with multivariate curve resolution. *Anal Chim Acta* 814:23–30. doi:10.1016/j.aca.2014.01.034
- Bakırcı GT, Yaman Acay DB, Bakırcı F, Ötleş S (2014) Pesticide residues in fruits and vegetables from the Aegean region, Turkey. *Food Chem* 160:379–392. doi:10.1016/j.foodchem.2014.02.051
- Bilehal DC, Chetti MB, Sung DD, Goroji PT (2014) Reversed-phase UPLC Method for the determination of monocrotophos, thiram, carbendazim, carbaryl and imidacloprid pesticides in mango and pomegranate by QuEChERS method. *J Liq Chromatogr Relat Technol* 37:1633–1643. doi:10.1080/10826076.2013.803205
- Zhan J, Yu X, Zhong Y, Zhang Z, Cui X, Peng J, Feng R, Liu X, Zhu Y (2012) Generic and rapid determination of veterinary drug residues and other contaminants in raw milk by ultra performance liquid chromatography–tandem mass spectrometry. *J Chromatogr B* 906:48–57. doi:10.1016/j.jchromb.2012.08.018
- Chen D, Tao Y, Liu Z, Liu Z, Lingli H, Wang Y, Yuanhu P, Peng D, Dai M, Yuan Z (2010) Development of a high-performance liquid chromatography method to monitor the residues of benzimidazoles in bovine milk. *J Chromatogr B* 878:2928–2932. doi:10.1016/j.jchromb.2010.08.029
- Razzino CA, Sgobbi LF, Canevari TC, Cancino J, Machado SAS (2015) Sensitive determination of carbendazim in orange juice by electrode modified with hybrid material. *Food Chem* 170:360–365. doi:10.1016/j.foodchem.2014.08.085
- Yao Y, Wen Y, Zhang L, Wang Z, Zhang H, Xu J (2014) Electrochemical recognition and trace-level detection of bactericide carbendazim using carboxylic group functionalized poly(3,4-ethylenedioxythiophene) mimic electrode. *Anal Chim Acta* 831:38–49. doi:10.1016/j.aca.2014.04.059
- Luo S, Wu Y, Gou H (2013) A voltammetric sensor based on GO–MWNTs hybrid nanomaterial-modified electrode for determination of carbendazim in soil and water samples. *Ionics* 19:673–680. doi:10.1007/s11581-013-0868-3
- Ribeiro WF, Selva TMG, Lopes IC, Coelho ECS, Lemos SG, Abreu FC, Nascimento VB, Araújo MCU (2011) Electroanalytical determination of carbendazim by square wave adsorptive stripping voltammetry with a multiwalled carbon nanotubes modified electrode. *Anal Methods* 3:1202. doi:10.1039/c0ay00723d
- Sundari PA, Palaniappan S, Manisankar P (2010) Enhanced sensing of carbendazim, a fungicide on functionalized multi-walled carbon nanotube modified glassy carbon electrode and its determination in real samples. *Anal Lett* 43:1457–1470. doi:10.1080/00032710903502066
- Li J, Chi Y (2009) Determination of carbendazim with multi-walled carbon nanotubes-polymeric methyl red film modified electrode. *Pestic Biochem Physiol* 93:101–104. doi:10.1016/j.pestbp.2008.12.004
- Guo Y, Guo S, Li J et al (2011) Cyclodextrin–graphene hybrid nanosheets as enhanced sensing platform for ultrasensitive determination of carbendazim. *Talanta* 84:60–64. doi:10.1016/j.talanta.2010.12.007
- Manisankar P, Selvanathan G, Vedhi C (2005) Utilization of sodium montmorillonite clay-modified electrode for the determination of isoproturon and carbendazim in soil and water samples. *Appl Clay Sci* 29:249–257. doi:10.1016/j.clay.2005.01.006
- Manisankar P, Selvanathan G, Vedhi C (2006) Determination of pesticides using heteropolyacid montmorillonite clay-modified electrode with surfactant. *Talanta* 68:686–692. doi:10.1016/j.talanta.2005.05.021
- França RF, de Oliveira HPM, Pedrosa VA, Codognoto L (2012) Electroanalytical determination of carbendazim and fenamiphos in natural waters using a diamond electrode. *Diam Relat Mater* 27–28:54–59. doi:10.1016/j.diamond.2012.05.010
- Rao TN, Sarada BV, Terashima C, Fujishima A (2002) Electrochemical detection of carbamate pesticides at conductive diamond electrodes. *Anal Chem* 74:1578–1583. doi:10.1021/ac010935d
- Khare NG, Dar RA, Srivastava AK (2015) Determination of carbendazim by adsorptive stripping differential pulse voltammetry employing glassy carbon paste electrode modified with graphene and amberlite XAD 2 resin. *Electroanalysis*. doi:10.1002/elan.201500080
- Noyrod P, Chailapakul O, Wonsawat W, Chuanuwatanakul S (2014) The simultaneous determination of isoproturon and carbendazim pesticides by single drop analysis using a graphene-

- based electrochemical sensor. *J Electroanal Chem* 719:54–59. doi:10.1016/j.jelechem.2014.02.001
19. Švancara I, Vytřas K, Kalcher K, Walcarus A, Wang J (2009) Carbon paste electrodes in facts, numbers, and notes: a review on the occasion of the 50-years jubilee of carbon paste in electrochemistry and electroanalysis. *Electroanalysis* 21:7–28. doi:10.1002/elan.200804340
 20. Hernandez P, Ballesteros Y, Galan F, Hernandez L (1996) Determination of carbendazim with a graphite electrode modified with silicone OV-17. *Electroanalysis* 8:941–946. doi:10.1002/elan.1140081018
 21. Ashrafi AM, Đorđević J, Guzsvány V, Švancara I, Trtić-Petrović T, Purenović M, Vytřas K (2012) Trace determination of carbendazim fungicide using adsorptive stripping voltammetry with a carbon paste electrode containing tricresyl phosphate. *Int J Electrochem Sci* 7:9717–9731
 22. Ya Y, Wang T, Xie L, Zhu J, Tang L, Ning D, Yan F (2015) Highly sensitive electrochemical sensor based on pyrrolidinium ionic liquid modified ordered mesoporous carbon paste electrode for determination of carbendazim. *Anal Methods* 7:1493–1498. doi:10.1039/C4AY02748E
 23. Osteryoung JG, Osteryoung RA (1985) Square wave voltammetry. *Anal Chem* 57:101A–110A. doi:10.1021/ac00279a789
 24. Lovrić M (2002) Square-wave voltammetry. In: Scholz PDF (ed) *Electroanal methods*. Springer, Berlin Heidelberg, pp 111–136
 25. Bard AJ, Faulkner LR (1980) *Electrochemical methods: fundamentals and applications*. Wiley, New York
 26. Lawrence NS, Beckett EL, Davis J, Compton RG (2002) Advances in the voltammetric analysis of small biologically relevant compounds. *Anal Biochem* 303:1–16. doi:10.1006/abio.2002.5584
 27. Lovrić M, Komorsky-Lovrić Š (1988) Square-wave voltammetry of an adsorbed reactant. *J Electroanal Chem Interfacial Electrochem* 248:239–253. doi:10.1016/0022-0728(88)85089-7
 28. Van Benschoten JJ, Lewis JY, Heineman WR, Roston DA, Kissinger PT (1983) Cyclic voltammetry experiment. *J Chem Educ* 60:772. doi:10.1021/ed060p772
 29. Zoski CG (2007) *Handbook of electrochemistry*. Ed. Thonson, Las Cruces
 30. Liu C, Kong D, Guo H (2014) The morphology control of zeolite ZSM-5 by regulating the polymerization degree of silicon and aluminum sources. *Microporous Mesoporous Mater* 193:61–68. doi:10.1016/j.micromeso.2014.03.015
 31. Kaur B, Srivastava R (2014) Selective, nanomolar electrochemical determination of environmental contaminants dihydroxybenzene isomers found in water bodies using nanocrystalline zeolite modified carbon paste electrodes. *Electroanalysis* 26:1739–1750. doi:10.1002/elan.201400171
 32. Liu X, Wang Y, Cui X, He Y, Mao J (2013) Influence of synthesis parameters on NaA zeolite crystals. *Powder Technol* 243:184–193. doi:10.1016/j.powtec.2013.03.048
 33. Simon U, Franke ME (2000) Electrical properties of nanoscaled host/guest compounds. *Microporous Mesoporous Mater* 41:1–36. doi:10.1016/S1387-1811(00)00291-2
 34. Abbaci A, Azzouz N, Bouznit Y (2014) A new copper doped montmorillonite modified carbon paste electrode for propineb detection. *Appl Clay Sci* 90:130–134. doi:10.1016/j.clay.2013.12.036
 35. Mozgawa W, Sitarz M, Rokita M (1999) Spectroscopic studies of different aluminosilicate structures. *J Mol Struct* 511–512:251–257. doi:10.1016/S0022-2860(99)00165-9
 36. Fernández-Jiménez A, Palomo A (2005) Mid-infrared spectroscopic studies of alkali-activated fly ash structure. *Microporous Mesoporous Mater* 86:207–214. doi:10.1016/j.micromeso.2005.05.057
 37. Lee HJ, Kim YM, Kweon OS, Kim IJ (2007) Structural and morphological transformation of NaX zeolite crystals at high temperature. *J Eur Ceram Soc* 27:561–564. doi:10.1016/j.jeurceramsoc.2006.04.156
 38. Silverstein RM, Webster FX, de Aguiar PF, Alencastro RB (2000) *Identificação espectrométrica de compostos orgânicos*. Livros Técnicos e Científicos, Rio de Janeiro
 39. Zhou W, Zhao K-S (2008) Dielectric response and analysis of structural evolution of NaA zeolite with high pretreatment temperature. *J Phys Chem C* 112:15015–15021. doi:10.1021/jp802106q
 40. Chi Q, Gopel W, Ruzgas T, Gorton L, Heiduschka P (1997) Effects of pretreatments and modifiers on electrochemical properties of carbon paste electrodes. *Electroanalysis* 9:357–365
 41. Sabatani E, Rubinstein I (1987) Organized self-assembling monolayers on electrodes. 2. Monolayer-based ultramicroelectrodes for the study of very rapid electrode kinetics. *J Phys Chem* 91:6663–6669. doi:10.1021/j100311a021
 42. Royal Society of Chemistry (1987) Recommendations for the definition, estimation and use of the detection limit. *Analyst* 112:199–204. doi:10.1039/AN9871200199